doi.org/10.36721/PJPS.2026.39.9.254.1

Fe_3O_4 nanoparticles suppress osteosarcoma via macrophage reprogramming and the MIP-1α-CCL3 axis

Zhangfan Gong and Yiran Yin*
Department of Orthopedics, The Affiliated Hospital of Southwest Medical University, Luzhou, Sichuan, China

Abstract: **Background**: Fe_3O_4 nanoparticles possess bone-targeting properties. This study investigated the anti-osteosarcoma mechanism of Fe_3O_4 nanoparticles by focusing on the tumor microenvironment, specifically examining their impact on macrophage activation. **Objectives**: To investigate their mechanism against osteosarcoma, focusing on the tumor microenvironment and specifically examining their impact on macrophage activation. **Methods**: The nanomaterials were characterized by electron microscopy and their release profiles were assessed both *in-vitro* and *in-vivo*. The antitumor activity of iron oxide nanoparticles (IONPs) was evaluated in osteosarcoma cell lines and mouse models by measuring tumor volume and size. Cytokine and inflammatory factor changes were analyzed using PCR-array and further validated by RT-PCR and Western blot. **Results**: All particles were within the size range of 11-17 nm with a normal distribution. Treatment with iron oxide nanoparticles significantly inhibited tumor cell proliferation, extended mouse survival and rescued macrophage activation in the tumor microenvironment. This mechanism is likely attributed to the reprogramming of macrophage activation and the activation of the MIP-1α/CCL3 signaling pathway. **Conclusion**: Fe_3O_4 nanoparticles effectively inhibit osteosarcoma progression by reprogramming macrophages and activating the MIP-1α/CCL3 signaling pathway, providing a new direction for developing nanotechnology-based immunotherapy strategies for osteosarcoma.

Keywords: Ferric oxide; MIP-1α/CCL3; Nanoparticles; Osteosarcoma

Submitted on 06-08-2025 – Revised on 01-12-2025 – Accepted on 09-12-2025

INTRODUCTION

Osteosarcoma is a highly malignant bone tumor that predominantly affects children and adolescents. Despite multimodal treatments, including surgery and intensive chemotherapy, the five-year survival rate has plateaued at approximately 60%, indicating a poor prognosis (Xu *et al*., 2024). A major challenge in the treatment of osteosarcoma is the high incidence of metastasis. Approximately 20% of patients present with radiologically detectable metastases at diagnosis, while up to 80% harbor undetectable micrometastases (Zhao *et al*., 2024; Nasir *et al*., 2022). Although surgery and adjuvant chemotherapy have improved overall survival in localized osteosarcoma, the survival rates for patients with metastatic or recurrent disease have remained low over the past few decades, with a post-relapse five-year survival rate of less than 30% (Yu and Yao, 2024; Liu *et al*., 2022). The clinical benefits of traditional chemotherapy are limited due to low tumor drug deposition and dose-limiting toxicities (Jiang *et al*., 2022; Adewuyi *et al*., 2025). Therefore, the development of novel drug delivery modalities and therapeutic strategies is urgently needed.

The malignant progression and drug resistance of tumors are closely associated with their complex tumor microenvironment (TME). In osteosarcoma, the TME is composed of various cell types, among which tumor-associated macrophages (TAMs) play a critical role (Zhao *et al*., 2021). TAMs typically exhibit plasticity, polarizing mainly between the pro-inflammatory M1 phenotype and the anti-inflammatory, pro-tumorigenic M2 phenotype. A high density of M2-type or "alternatively activated" TAMs is associated with poor prognosis in various cancers (Zhao *et al*., 2021). M2 macrophages exert immunosuppressive functions by secreting immunosuppressive factors, whereas M1 macrophages participate in inflammatory responses through the secretion of pro-inflammatory factors (Anand *et al*., 2023). In a viral myocarditis model, the lncRNA AK083884, derived from M2 macrophage exosomes, was shown to mediate metabolic reprogramming in macrophages by regulating the PKM2/HIF-1α axis, influencing disease progression (Zhang *et al*., 2024). Similarly, in osteosarcoma, molecules such as TMEM64 (Yang *et al*., 2024) and the m6A-modified lncRNA CHASERR (Wu *et al*., 2024) have been demonstrated to exacerbate the malignant phenotype by activating signaling pathways like Wnt/β-catenin, indicating extremely complex signal crosstalk within the TME. Furthermore, the mechanisms of drug resistance in osteosarcoma are intricate. Studies have revealed that the dual regulation of Sprouty 4 palmitoylation by ZDHHC7 and palmitoyl-protein thioesterase 1 provides a potential therapeutic strategy to overcome cisplatin resistance (Huang *et al*., 2025). Recent research in sarcoma has also highlighted the potential role of liquid-liquid phase separation in pathogenesis and treatment (Cheng *et al*., 2025).

In recent years, the application of nanomaterials in the biomedical field, particularly in targeted drug delivery, has shown significant potential (Xu *et al*., 2023; Park *et al*., 2022). Among them, iron oxide (Fe_3O_4) nanoparticles have garnered considerable attention due to their good

**Corresponding author:* e-mail: yiranyin@swmu.edu.cn

biocompatibility, superparamagnetism, ease of surface functionalization and inherent bone-targeting properties (Zheng *et al*., 2021; Zhang *et al*., 2024). These nanoparticles can serve as carriers to specifically deliver chemotherapeutic drugs, genetic material, or immunomodulators to tumor sites, thereby enhancing therapeutic efficacy and reducing systemic toxicity. The design of nanomaterials has also become increasingly sophisticated. Studies indicate that small-molecule drugs such as dimethyl fumarate can enhance the anticancer activity of nanoparticles (e.g., silver nanoparticles) by activating pathways like NRF2 (Stephens *et al*., 2025), offering new avenues for combining nanotechnology with osteosarcoma treatment. Although antitumor mechanisms of Fe_3O_4 nanoparticles, such as their photothermal effect, have been reported (Li *et al*., 2024), the specific molecular mechanisms by which they influence osteosarcoma progression through modulation of the tumor microenvironment, particularly the polarization state of macrophages, remain unclear.

This study aims to investigate the impact of Fe_3O_4 nanoparticles on osteosarcoma and specifically examine whether their mechanism of action involves influencing macrophage activation within the tumor microenvironment. We hypothesize that Fe_3O_4 nanoparticles may modulate key signaling pathways, such as MIP-1α/CCL3, thereby affecting the functional state of macrophages, altering the immune landscape of the TME and ultimately inhibiting osteosarcoma growth. This research will not only help elucidate a novel mechanism of Fe_3O_4 nanoparticles but also provide a theoretical foundation for developing new nanotechnology-based immunotherapeutic strategies for osteosarcoma.

MATERIALS AND METHODS

Animal feeding

Ctsk-Ctrl and Ctsk-CKO mice (C57BL/6J background) were obtained from The Jackson Laboratory (Bar Harbor, ME, USA) and subsequently bred in the animal facility of The Affiliated Hospital of Southwest Medical University. All mice were maintained under specific pathogen-free (SPF) conditions in individually ventilated cages (IVCs), with regular health monitoring. Both male and female mice were used in this study, with equal sex distribution per group (n = 3–4 males and 3–4 females per group, totaling 7 mice per group). At the start of the experiment (8 weeks of age), body weight ranged from 20 to 25 g, with no significant differences among groups. Mice were housed under standard indoor conditions at 23 ± 1°C and 55–60% humidity, with a 12-hour light/dark cycle. They were randomly assigned to four groups: Ctsk-Ctrl group, Ctsk-Ctrl+Fe_3O_4 nanoparticles group, Ctsk-CKO group, and Ctsk-CKO+Fe_3O_4 nanoparticles group. Mice (8 weeks old) were fed with water containing 100 μg/mL Fe_3O_4 nanoparticles for 12 weeks. Then, mice (20 weeks old) were humanely euthanized by inhalation of carbon dioxide (CO_2) followed by cervical dislocation, in accordance with the AVMA Guidelines for the Euthanasia of Animals. Death was confirmed by cessation of heartbeat and respiration. The number of mice per group (n = 7) was determined based on pre-experimental data and calculated using G*Power software (α = 0.05, β = 0.2, effect size d = 1.5) to ensure a statistical power of ≥80%. Exclusion criteria were predefined as follows: (1) unexpected death before the scheduled endpoint due to causes unrelated to treatment; (2) failure to develop measurable tumors; (3) signs of severe systemic illness (e.g., >20% body weight loss, severe lethargy). No mice met these exclusion criteria during the study. All animal experimental procedures strictly adhered to the institution's "Guidelines for the Care and Use of Laboratory Animals" (Storves *et al*., 2025) and were approved by the Animal Ethics Committee of The Affiliated Hospital of Southwest Medical University (Approval No: AHSMU-E-20240505).

Nanoparticle construction

20 mg of HMNPs and 80 mg of PU-TMP were co-dissolved in 2.8 g of chloroform ($CHCl_3$). Subsequently, 5 mL of a sodium dodecyl sulfate (SDS, 0.6 mg/mL) solution was added and the mixture was subjected to ultrasonic emulsification at 200 W power for 10 minutes in an ice bath to form a microemulsion. Chloroform was then removed via evaporation until no chloroform volatilization was detected, resulting in a deep-yellow PTCP-20 latex (with an HMNPs content of 20%). The prepared Fe_3O_4 nanoparticles were surface-coated with oleic acid via coordination to render them hydrophobic.

Tissue staining

To examine the tissues, paraffin sections were stained with 0.1% Sirius Red F3B and 1.3% picric acid or Masson's trichrome saturated aqueous solution to assess collagen deposition. Ten non-overlapping areas per section (n = 7) were scored semi-quantitatively, relative to total area. The tissue samples were dehydrated and fixed for section processing, and the cytological morphology was stained with hematoxylin and eosin (H&E) (Lorsuwannarat *et al*., 2024), and cell morphology was observed under a microscope. Inflammatory cell markers were analyzed by immunofluorescence (IF) microscopy. Positive signals in IF images were quantified from at least five randomly selected regions using ImageJ 1.52 software.

Immunohistochemical staining

After slides were treated for 60 min, the primary antibody (1:100, Abcam) was applied for 1 h incubation. After secondary antibody staining, slides were counterstained with hematoxylin and then with blue reagent.

RT-PCR

RNA was extracted from miRNeasy FFPE using TransScript Green One-Step qRT-PCR SuperMix (Shanghai Thermo Fisher Co., Ltd.). TM microRNA qPCR Quantification Kit (Galimberti *et al*., 2022).

Table 1: Real-time PCR primers and primer sequences.

Primer		Sequences
smMHC	Forward primer	5'-ACGCTGGTGCTCTATGCAAG-3'
	Reverse primer	5'-ACGCTGGTGCTCTATGCAAG-3'
CD31	Forward primer	5'-GACTCTTGCGTCAACTTCAAGG-3'
	Reverse primer	5'-CAGGCTGTCTTTTGTCAACGA-3'
GAPDH	Forward primer	5'-AAAGGGTCATCATCTCCGCC-3'
	Reverse primer	5'-AGTGATGGCATGGACTGTGG-3'
MIP-1α	Forward primer	F: 5'-ATTACCCGCCCGAGAAAGG-3'
	Reverse primer	R: 5'-TCGCAGCAAAGATCCACACAG-3'
Caspase-1	Forward primer	F: 5'-CTTGGAGACATCCTGTCAGGG-3'
	Reverse primer	R: 5'-AGTCACAAGACCAGGCATATTCT-3'

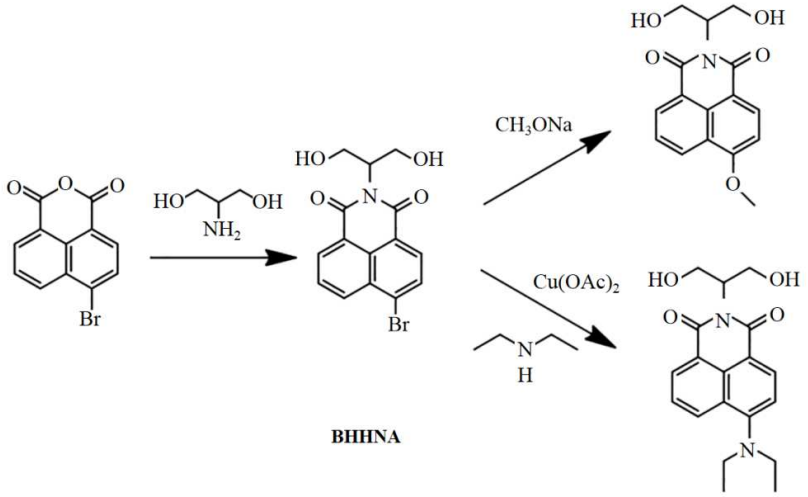

Fig. 1: Molecular formula of Fe_3O_4 nanoparticles.

GAPDH was used as a control and the real-time PCR was performed using the total cDNA as the starting material on a real-time PCR system (Shanghai Thermo Fisher Co., Ltd.). Software analysis. The primer sequences used are listed in table 1.

Western blot

Protein was isolated and quantified followed by Western blot analysis using primary antibody (Proteintech, 1:1000). Protein bands were assessed by Odyssey Imaging System (Liu and Herr, 2024).

Immunofluorescence staining

Cells seeded in 6-well plates were transfected with the plasmid, it was washed twice with PBS, fixed with formalin and permeabilized with Triton-X100 solution. After blocking, the primary antibody was added for overnight incubation and the secondary antibody was added the next day and the blocking solution added. Then, 4,6-diamino-2-phenylindole was added for fixation, which was used for nuclear counterstaining and the protein was observed with a fluorescent microscope. Negative control photos were processed in a similar manner and PBS was used as a control.

Statistical analysis

Statistical analysis was performed using SPSS 19.0 software. Data are presented as mean ± standard deviation (SD). For in-vitro cell experiments, each treatment group consisted of at least six independent biological replicates ($n \geq 6$) to ensure statistical power and result reproducibility. For animal experiments, seven mice were used per group ($n = 7$) to ensure result reproducibility and statistical robustness. Comparisons among multiple groups were assessed by one-way analysis of variance (ANOVA), followed by Tukey's post hoc test for multiple comparisons. Survival curves were plotted using the Kaplan-Meier method and differences between groups were analyzed by the Log-rank test. For the primary outcome (tumor volume), effect sizes were calculated as Cohen's d using G*Power software. A Cohen's d value >0.8 was considered a large effect size. A P-value <0.05 was considered statistically significant.

Blinding: All outcome assessments, including tumor volume measurement, histological scoring (HE, PCNA, TUNEL, and immunofluorescence staining), Western blot band quantification, and RT-PCR data analysis, were performed by investigators blinded to the group allocation. Unblinding occurred only after all data had been collected and analyzed.

RESULTS

Preparation of Fe_3O_4 nanoparticles

The surface coating coordinated by oleic acid renders the magnetic nanoparticles hydrophobic. Observation by transmission electron microscope shows that ferric oxide nanoparticles are relatively uniform and spherical. It can be seen that the size of ferroferric oxide nanoparticles is mostly in 11-17 nm (Fig. 2A) with normal distribution (Fig. 2B). In FT-IR spectrum (Fig. 2C), absorption peaks at 2923 and 2850 cm−1 are saturated C-h stretching, indicating that the Fe_3O_4 nanoparticles are composed of magnetite and oleic acid (Fig. 2D). DLS results showed a PDI of 0.12 and a Zeta potential of -25.3 mV, indicating that the nanoparticles possess good colloidal stability.

Fe_3O_4 nanoparticles improve osteosarcoma in mice

To investigate the role of Fe_3O_4 nanoparticles in osteosarcoma progression, we performed HE and PCNA staining and found significantly attenuated proliferation of tumor cells after treatment with Fe_3O_4 nanoparticles (Fig. 3A). In contrast, the survival period of mice after treatment with Fe_3O_4 nanoparticles was significantly prolonged, as shown in Fig. 3B.

Activation of macrophages in the tumor microenvironment of osteosarcoma mice was improved by Fe_3O_4 nanoparticles

Fig. 4A and 4B show significantly increased caspase-1 levels and TUNEL positive cells in mice fed with Fe_3O_4 nanoparticles. The activation of caspase-1 in HFD mice treated with ferric oxide nanoparticles was enhanced (Fig. 4C). As shown in fig. 4D and 4E, CD31 was highly enriched in the tumor tissue, but the expression of CD31 was hardly detected around the tumor (*P=0.012). On the contrary, the expression of smMHC in the tumor tissue was low and the expression was high in the periphery of the tumor, indicating that the isolated RNA mainly came from macrophages.

Effect of loss of M1 expression on the expression of tumor inflammatory factors

As shown in fig. 5A, the expression of CCL2 (2.41-fold), TSLP (2.17-fold), CSF2 (2.26-fold), CCL5 (2.05-fold), CCL3 (2.59-fold) and MIP-1α (2.74-fold) was significantly upregulated. mRNA was extracted from tumor tissues of two induced mouse groups (Ctsk- Ctrl and Ctsk-Ctrl+Fe_3O_4 nanoparticles mice) for RT-PCR verification, also found that MIP-1α and CCL3 expression in Ctsk-Ctrl+Fe_3O_4 nanoparticles mice were significantly up-regulated, Fig. 5B. And there is a statistical difference (**P=0.000).

Ctsk-Ctrl+Fe_3O_4 nanoparticles mice activate MIP-1α/CCL3 signaling

MIP-1α and CCL3 were up-regulated and there was a statistical difference (Fig. 6A). In Fig. 6B, their membrane expression was also significantly enhanced after induction treatment. The results showed that the specific inhibition of M1 expression in macrophages promoted the activation of MIP-1α/CCL3 and increased the phenotypic transformation of vascular smooth muscle cells. Detecting CD31 staining expression to evaluate vascular remodeling, fig. 6C, after adding MIP-1α recombinant protein to tumor MG63 cells, the cells gradually developed into a spindle shape and grew in a swirl shape; CD31 staining results showed that after adding MIP-1α recombinant protein, blood vessels were increased. So it affects the activation of tumor cells after activating MIP-1α/CCL3 signaling.

DISCUSSION

In this study, ferric oxide nanoparticles were successfully prepared to interfere with the development of osteosarcoma cells. Fe_3O_4 nanoparticles are a type of nanoparticle that can treat tumors through the photothermal effect (Li *et al*., 2024). However, there are few reports on its mechanism. Compared to the triggered luminescence characteristics of polypeptide nanoparticles (Gao *et al*., 2025), Fe_3O_4 nanoparticles demonstrate unique advantages in the targeted therapy of osteosarcoma due to their inherent bone-targeting properties, superparamagnetism and favorable biocompatibility. Therefore, they have potential applications as controlled-release drug carriers (Shen *et al*., 2021; Song *et al*., 2026). A key finding of this study is that Fe_3O_4 nanoparticles can modulate the activation state of macrophages within the tumor microenvironment of osteosarcoma-bearing mice and activate the MIP-1α/CCL3 signaling pathway. To ensure the reliability of this critical conclusion, all in vitro experiments investigating this pathway were conducted with at least six independent biological replicates. The consistent results across these replicates significantly enhance the statistical power of the data and the robustness of the conclusion.

The analysis in this study aligns with the perspective that inflammatory signaling pathways in the tumor microenvironment are critically important. Previous studies have indicated (Shi *et al*., 2025) that the canonical NF-κB pathway, activated by inflammatory factors such as IL-1 and TNF, plays a critical role in regulating the expression of genes associated with inflammation, cell proliferation, survival, and metastasis, highlighting the direct driving effect of the canonical NF-κB pathway on osteosarcoma progression. In contrast, our research identified that Fe_3O_4 nanoparticles exert their anti-tumor effects through another related inflammatory pathway – MIP-1α/CCL3. As an important chemokine, MIP-1α/CCL3 functions in recruiting and activating immune cells, including macrophages. This study observed that the upregulation of this pathway coincided with a tumor-suppressive phenotype, suggesting that Fe_3O_4 nanoparticles may combat the tumor by remodeling the immune microenvironment rather than through direct cell killing.

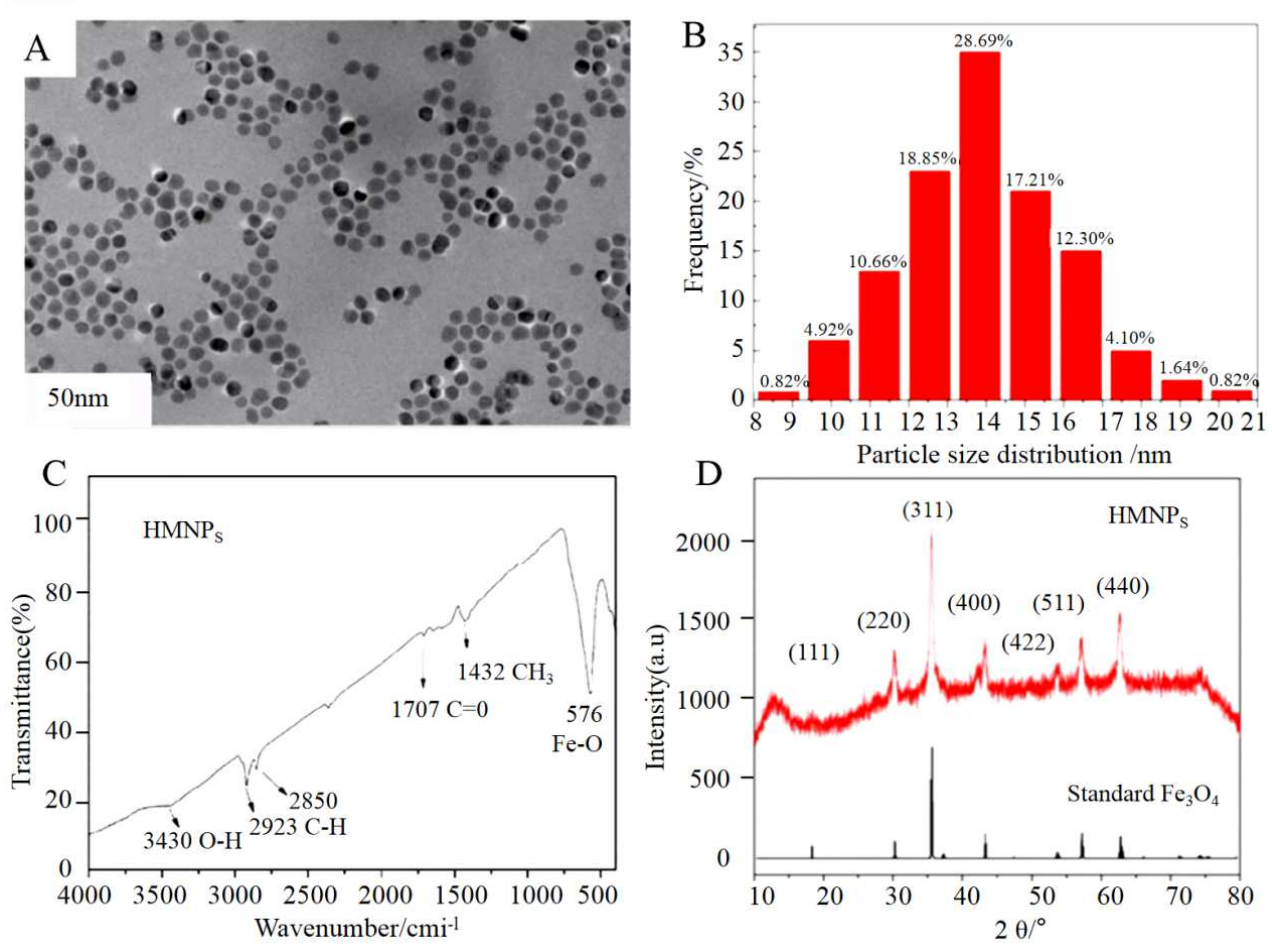

Fig. 2: Preparation and characterization of Fe_3O_4 nanoparticles. (A) Transmission electron microscopy (TEM) image showing particle morphology and size. Scale bar: 50 nm; (B) Zeta potential distribution of Fe_3O_4 nanoparticles; (C) FT-IR spectrum of Fe_3O_4 nanoparticles. Y-axis: Transmittance (%). Characteristic absorption peaks at 2923 cm^{-1} and 2850 cm^{-1} correspond to saturated C–H stretching, indicating oleic acid coating; (D) X-ray diffraction (XRD) pattern of Fe_3O_4 nanoparticles. Y-axis: Intensity (a.u.). The diffraction peaks are indexed to the cubic spinel structure of magnetite (Fe_3O_4).

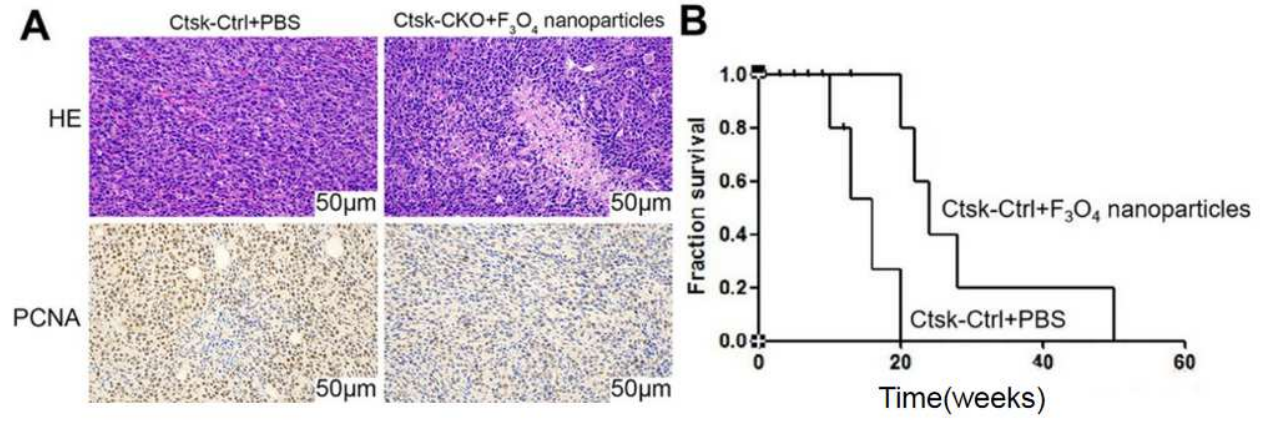

Fig. 3: Fe_3O_4 nanoparticles improve lesions in mice with osteosarcoma.
(A) HE and IHC staining, Scale bar: 100 μm; (B) Survival data of mice after different treatments.

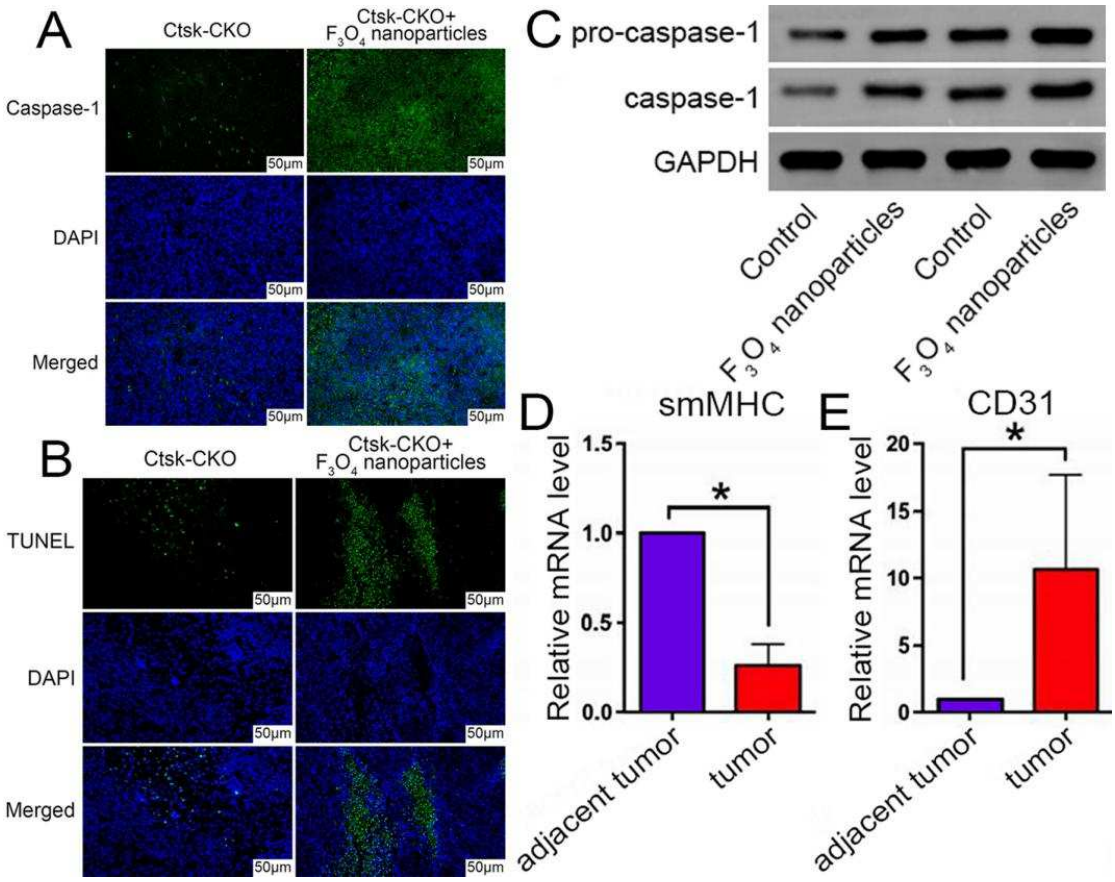

Fig. 4: The activation of macrophages in the tumor microenvironment of mice with osteosarcoma improved by Fe_3O_4 nanoparticles.
(A) Double immunofluorescence staining for CD31 (green) and activated caspase-1 (red, serving as a marker for M1-like macrophage-associated inflammatory state). Scale bar: 50 μm; (B) Double immunofluorescence staining for CD31 (green) and TUNEL (red, indicating apoptotic cells, with increased signal associated with the cytotoxic function of M1-like macrophages). Scale bar: 50 μm; (C) Western-blot detection of apoptotic protein expression; (D) RT-PCR detection of smMHC and CD31 expression in adjacent tumor and tumor tissues. *P=0.012.

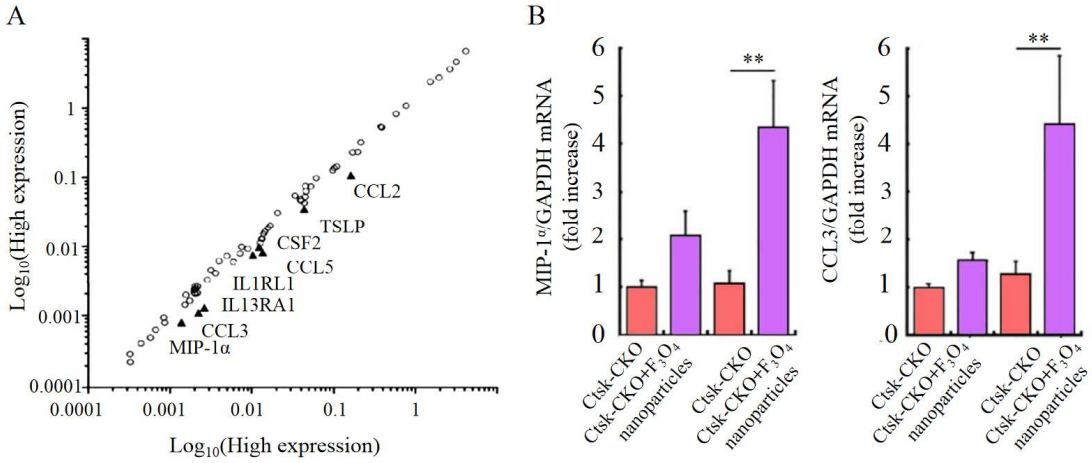

Fig. 5: The effect of loss of M1 expression on the expression of vascular inflammatory factors.
(A) The mRNA expression profile of cytokines in the tumor microenvironment following inhibition of the M1 macrophage phenotype was analyzed by PCR array. Each data point represents a gene, with its height corresponding to the fold change in its mRNA expression; (B) RT-PCR detection of MIP-1α and CCL3 mRNA levels; ** indicates P=0.000.

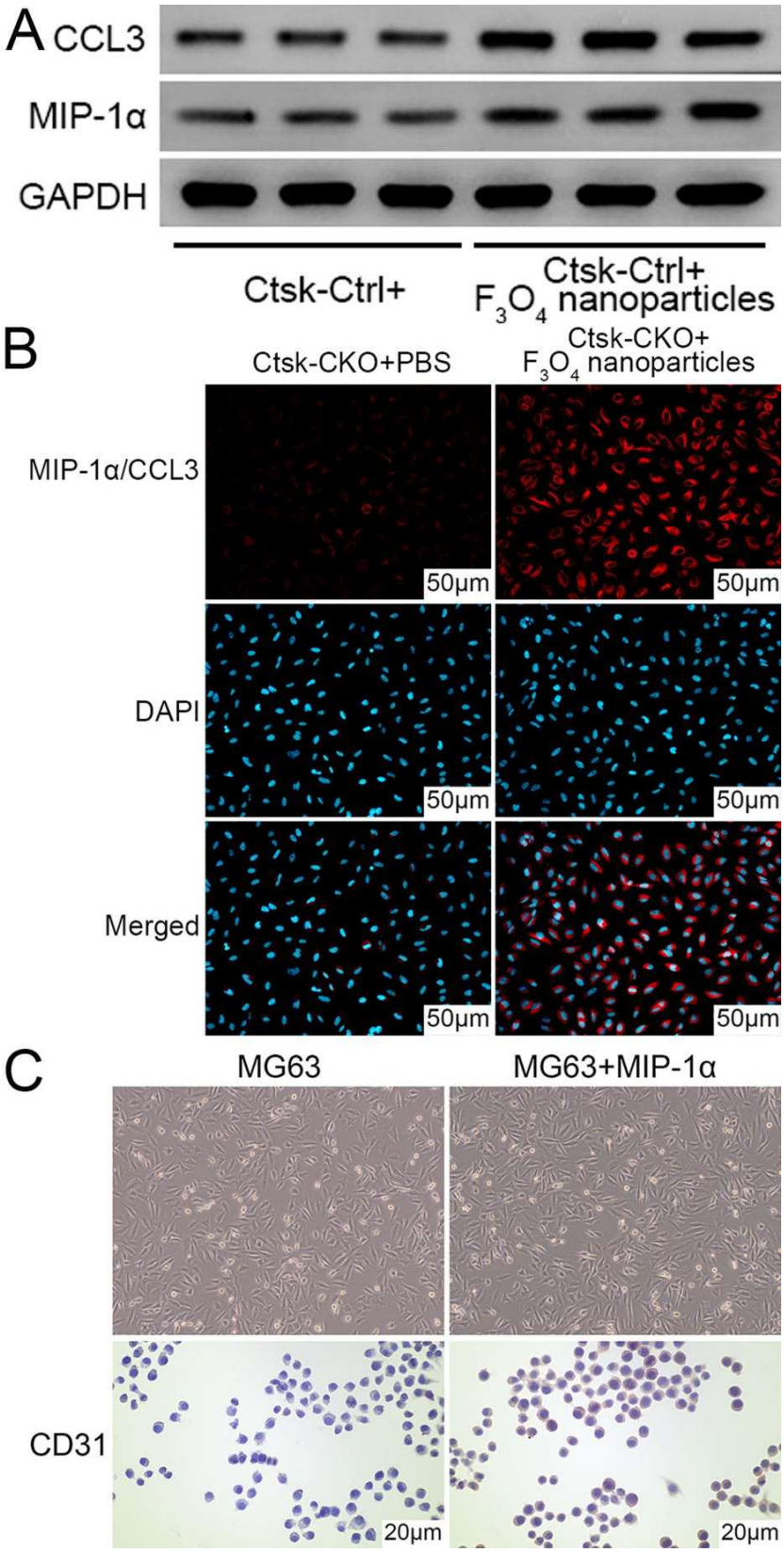

Fig. 6: Ctsk-Ctrl+ ferric oxide nanoparticle mice activate MIP-1α/CCL3 signaling pathway.
(A) Western-blot detection of the protein expression of MIP-1α and CCL3; (B) Immunofluorescence detection to compare the expression of MIP-1α/CCL3 on cells. Scale bar: 25 μm; (C) The effect of MIP-1α on tumor cells.

The analysis in this study aligns with the crucial role of inflammatory signaling pathways in the tumor microenvironment. Recent studies have demonstrated that Cyclovirobuxine D (CVB-D) suppresses osteosarcoma progression by inhibiting the non-canonical NF-κB pathway, reducing stemness markers such as ALDH1A1 and CD24, and inducing apoptosis (Guo *et al*., 2026), further supporting the crucial role of inflammatory signaling pathways in the tumor microenvironment. In comparison, our study demonstrates that Fe_3O_4 nanoparticles exert anti-tumor effects through another related inflammatory pathway—MIP-1α/CCL3. As an important chemokine, MIP-1α/CCL3 is involved in recruiting and activating immune cells, including macrophages. The observed upregulation of this pathway alongside a tumor-suppressive phenotype suggests that Fe_3O_4 nanoparticles combat tumors by remodeling the immune microenvironment rather than through direct cytotoxicity.

To evaluate the impact of Fe_3O_4 nanoparticles on macrophage activation in the tumor microenvironment, this study examined markers associated with inflammasome activation and apoptosis. Mice treated with Fe_3O_4 nanoparticles showed significantly increased levels of caspase-1 and TUNEL-positive cells in tumor tissues. Activated caspase-1 is a key executor of inflammasome activation in M1-like macrophages, driving the maturation of pro-inflammatory cytokines IL-1β and IL-18. Furthermore, partial co-localization of TUNEL-positive cells with the macrophage marker F4/80 was observed, suggesting that activated macrophages may exert anti-tumor effects by inducing apoptosis in tumor cells. Thus, the elevated caspase-1 levels and increased TUNEL-positive cells collectively indicate a shift in the tumor microenvironment toward an anti-tumor, M1-like macrophage phenotype.

Although macrophage depletion experiments were not conducted in this study, numerous recent studies has established the central role of macrophages in nanomaterial-based therapy. Related research explicitly stated that polarizing macrophages from pro-tumoral M2 to anti-tumoral M1 phenotypes is an important strategy in cancer immunotherapy (Li *et al*., 2026). More importantly, recent osteosarcoma research. experimentally demonstrated that eliminating tumor-derived migrasomes suppresses M2 polarization of macrophages, thereby alleviating tumor progression (Liu *et al*., 2025), directly proving that modulating macrophage function can alter the malignant course of osteosarcoma. Based on this, our study proposes that Fe_3O_4 nanoparticles likely reprogram tumor-associated macrophages to reshape the immune landscape of the tumor microenvironment, with the observed upregulation of the MIP-1α/CCL3 pathway representing a key molecular manifestation of this reprogramming process.

This study not only confirms that Fe_3O_4 nanoparticles activate the MIP-1α/CCL3 signaling pathway but, more importantly, establishes a link between the activation of this pathway and macrophage reprogramming leading to a subsequent tumor-suppressive phenotype. A key scientific question arises: is the activation of the MIP-1α/CCL3 pathway a necessary condition for the anti-tumor effects of Fe_3O_4 nanoparticles? While direct loss-of-function experiments remain the gold standard for definitively answering this question, recent research in immunometabolism and inflammation provides strong logical support for our findings. In an acute liver injury model, Qiao *et al (2025)*. discovered that Rehmannia glutinosa polysaccharides can significantly alleviate LPS-induced inflammation and improve liver function by specifically inhibiting the TLR4/NF-κB and MAPK signaling pathways. This demonstrates that the precise modulation of overactivated inflammatory pathways is a viable therapeutic strategy. In a complementary finding within the field of tissue regeneration, recent research revealed the central role of the P2X7R/NLRP3 inflammasome axis in inhibiting enthesis regeneration. Blocking this axis effectively promoted tissue repair by remodeling the inflammatory and metabolic crosstalk between macrophages and stem cells (Gao *et al*., 2025). Collectively, these studies indicate that targeted intervention in specific immune-inflammatory signaling pathways can decisively influence the ultimate outcome of a disease.

Furthermore, this study evaluated changes in the tumor vasculature through CD31 staining. The results indicated an increase in CD31-positive signal areas within the tumor tissue following the addition of recombinant MIP-1α protein. CD31 is a classical marker for vascular endothelial cells and its upregulation is typically interpreted as an indication of angiogenesis. Considering the differential CD31 expression observed between the core and peripheral regions of the tumor in our in vivo experiments, the current data suggest that activation of the MIP-1α/CCL3 pathway may promote intra-tumoral angiogenesis, potentially representing a tumor response to microenvironmental changes. This vascular alteration coincided with a morphological shift of MG63 cells towards a more invasive spindle shape, collectively influencing tumor cell activation and the malignant phenotype. Consequently, we propose a plausible hypothesis: in the context of osteosarcoma, the MIP-1α/CCL3 signaling induced by Fe_3O_4 nanoparticles similarly plays a central role in driving anti-tumor immunity and blocking this pathway would likely reverse its therapeutic efficacy. This explicit hypothesis provides clear direction for future functional validation studies.

This study also has limitations. We did not investigate all subtypes of macrophages, which is a shortcoming of this work. In subsequent research, we will focus on examining

the phenotypes and mechanisms associated with other subtypes.

CONCLUSION

In conclusion, our study revealed that the proliferation of tumor cells was significantly attenuated after Fe3O4 nanoparticle treatment; in contrast, the survival time of mice treated with Fe_3O_4 nanoparticles was significantly prolonged. At the same time, ferric oxide nanoparticles improved macrophage activation in tumor microenvironment of osteosarcoma mice. It is suggested that Fe_3O_4 nanoparticles can slow down the proliferation of osteosarcoma by activating the expression of MIP-1α/CCL3 signal and have a significant anti-tumor effect in tumors.

Acknowledgements
None

Authors' contributions
Zhangfan Gong and Yiran Yin: Conceptualization, data curation, formal analysis, writing - original draft; Zhangfan Gong: Investigation, data curation; Yiran Yin: Supervision, writing - review and editing; Yiran Yin: Resources, methodology. All authors have read and approved the final manuscript.

Funding
There was no funding.

Data availability statement
The datasets generated and/or analyzed during the current study are available from the corresponding author on reasonable request.

Ethical approval
All animal experimental procedures were strictly conducted in accordance with the institutional Guide for the Care and Use of Laboratory Animals and internationally recognized ethical standards for animal research (e.g., ARRIVE guidelines). The study protocol was reviewed and approved by the Clinical Trial Ethics Committee of The Affiliated Hospital of Southwest Medical University (KY2025305). All efforts were made to minimize the suffering and the number of animals used. This study was performed in adherence with the ARRIVE guidelines. See supplementary file for the ARRIVE checklist.

Conflict of interest
The authors declare that the research was conducted in the absence of any commercial or financial relationships that could be construed as a potential conflict of interest.

Supplementary data
https://www.pjps.pk/uploads/2026/06/SUP1781433398.pdf

REFERENCES

Adewuyi E, Chorya H, Muili A, Moradeyo A, Kayode A, Naik A, Odedele T and Opabode M (2025). Chemotherapy, immunotherapy and targeted therapy for osteosarcoma: Recent advancements. *Crit Rev Oncol Hematol*., **206**: 104575.

Anand N, Peh KH and Kolesar JM (2023). Macrophage repolarization as a therapeutic strategy for osteosarcoma. *Int J Mol Sci*., **24**(3): 2858.

Cheng Z, Wang H, Zhang Y, Ren B, Fu Z, Li Z and Tu C (2025). Deciphering the role of liquid-liquid phase separation in sarcoma: Implications for pathogenesis and treatment. *Cancer Lett*., **616**: 217585.

Gao H, Wang L, Lyu Y, Jin H, Lin Z, Kang Y, Li Z, Zhang X, Jiang Y, Zhang G, Tao Z, Zhang X, Yang B, Bai X, Ma X, Liu S and Jiang, J (2025). The P2X7R/NLRP3 inflammasome axis suppresses enthesis regeneration through inflammatory and metabolic macrophage-stem cell cross-talk. *Sci Adv*., **11**(17): 4894.

Gao Y, Wang Y, Jiang J, Wei P and Sun H (2025). Triggered "On/off" luminescent polypeptide bowl-shaped nanoparticles for selective lighting of tumor cells. *Small*., **21**(11): e2411432.

Galimberti S, Balducci S, Guerrini F, Del Re M and Cacciola R (2022). Digital droplet PCR in hematologic malignancies: A new useful molecular tool. *Diagnostics (Basel)*., **12**(6): 1305.

Guo J, Cao Y, Jin K, Liu B, Wang W, Chen C and Xie J, Xu A (2026). Cyclovirobuxine D suppresses cancer stemness in osteosarcoma with implication of the noncanonical NF-kappaB pathway. *Front Pharmacol*., **17**: 1746984.

Huang T, Chen Y, Zhao Q, Wu X, Li H, Luo X, Su Y, Zhang S, Liu P and Tang N (2025). Dual regulation of sprouty 4 palmitoylation by ZDHHC7 and palmitoyl-protein thioesterase 1: A potential therapeutic strategy for cisplatin-resistant osteosarcoma. *Research (Wash DC)*., **8**: 0708.

Jiang J, Wang R, Yang L, Sha Y, Zhao S, Guo J, Chen D, Zhong Z and Meng F (2022). IL-11Rα-targeted nanostrategy empowers chemotherapy of relapsed and patient-derived osteosarcoma. *J Control Release*., **350**: 460–470.

Li Y, Chen J, Xia Q, Shang J, He Y, Li Z, Chen Y, Gao F, Yu X, Yuan Z and Yin P (2024). Photothermal Fe_3O_4 nanoparticles induced immunogenic ferroptosis for synergistic colorectal cancer therapy. *J Nanobiotechnology*., **22**(1): 630.

Li H, Liu C, Zhang B, Zhang Y and Liu Y (2026). Macrophage plasticity in the osteosarcoma tumor microenvironment: opportunities and challenges for immunotherapy. *J Cancer Res Clin Oncol*., **152**(4): 88.

Liu W, Li L, Bai X, Zhang M, Lv W, Ma Y, Sun Y, Zhang H, Jiang Q, Yao Q and Zhang ZY (2025). Osteosarcoma cell-derived migrasomes promote macrophage m2 polarization to aggravate osteosarcoma proliferation and

metastasis. *Adv Sci (Weinh)*., **12**(17): e2409870.

Liu Z, Yin J Zhou Q Yang J, Zeng B, Yeung SJ, Shen J and Cheng C (2022). Survival after pulmonary metastasectomy for relapsed osteosarcoma. *J Thorac Cardiovasc Surg*., **163**(2): 469–479.e8.

Liu Y and Herr AE (2024). DropBlot: Single-cell western blotting of chemically fixed cancer cells. *Nat Commun*., **15**(1): 5888.

Lorsuwannarat N, Kaewsanit A, Charoenpitakchai M, Ruangpratheep C, Arnutti P and Nimmanon T (2024). Optimizing re-staining techniques for the restoration of faded hematoxylin and eosin-stained histopathology slides: A comparative study. *J Histochem Cytochem*., **72**(11-12): 733–742.

Nasir MU, Khan S, Mehmood S, Khan MA, Rahman AU and Hwang SO (2022). IoMT-Based osteosarcoma cancer detection in histopathology images using transfer learning empowered with blockchain, fog computing and edge computing. *Sensors (Basel)*., **22**(14): 5444.

Park H, Otte A and Park K (2022). Evolution of drug delivery systems: From 1950 to 2020 and beyond. *J Control Release*., **342**: 53–65.

Qiao H, Ren H, Liu Q, Jiang Y, Wang Q, Zhang H, Gan L, Wang P, Cui Y, Wang J, Chou Y, Chen L, Shi J and Dou Y (2025). Anti-inflammatory effects of Rehmannia glutinosa polysaccharide on LPS-induced acute liver injury in mice and related underlying mechanisms. *J Ethnopharmacol*., **351**: 120099.

Shen JY, Dong T, Fang L, Ma JJ and Zeng LH (2021). Study on multifunctional composite nanomaterials for controlled drug release in biomedicine. *J Nanosci Nanotechnol*., **21**(2): 1230–1235.

Shi S, Ou X, Liu C, Li R, Zheng Q and Hu L (2025). NF-κB signaling and the tumor microenvironment in osteosarcoma: implications for immune evasion and therapeutic resistance. *Front Immunol*., **16**:1518664.

Song JB, Li JY, Ding YB, Yang SZ, Sun L, Yang Y, Lin ZX, Feng YC and Liu FX (2026). Research Progress of Ferrosoferric Oxide Nanoparticles in Bone Regeneration and Disease Treatment. *Int J Nanomedicine*., **21**: 570169.

Stephens E, Greenhough A and Mansell JP (2025). The Nrf2 inhibitor brusatol promotes human osteosarcoma (MG63) growth and blocks EB1089-induced differentiation. *Int J Mol Sci*., **26**(19): 9675.

Storves KP, Talcott MR, Wallace JM, Bennett BT, Makaron LM, Clemons D, Hugh Chip Price V, Cohen JK, Hasenau JJ, Freed C K and Leland SE (2025). The veterinary consortium for research animal care and welfare survey on revisions to the eighth edition of the guide for the care and use of laboratory animals. *J Am Assoc Lab Anim Sci*., **64**(4): 1–10.

Wu X, Fu M, Ge C, Zhou H, Huang H, Zhong M, Zhang M, Xu H, Zhu G, Hua W, Lv K and Yang H (2024). m6A-Mediated upregulation of lncRNA CHASERR promotes the progression of glioma by modulating the miR-6893-3p/TRIM14 Axis. *Mol Neurobiol*., **61**(8): 5418–5440.

Xu B, Li S, Shi R and Liu H (2023). Multifunctional mesoporous silica nanoparticles for biomedical applications. *Signal Transduct Target Ther*., **8**(1): 435.

Xu Y, Shi F, Zhang Y, Yin M, Han X, Feng J and Wang G (2024). Twenty-year outcome of prevalence, incidence, mortality and survival rate in patients with malignant bone tumors. *Int J Cancer*., **154**(2): 226–240.

Yang H, Zhou H, Fu M, Xu H, Huang H, Zhong M, Zhang M, Hua W, Lv K and Zhu G (2024). TMEM64 aggravates the malignant phenotype of glioma by activating the Wnt/β-catenin signaling pathway. *Int J Biol Macromol*., **260**(1): 129332.

Yu S and Yao X (2024). Advances on immunotherapy for osteosarcoma. *Mol Cancer*., **23**(1): 192.

Zhang Y, Zhu L, Li X, Ge C, Pei W, Zhang M, Zhong M, Zhu X and Lv K (2024). M2 macrophage exosome-derived lncRNA AK083884 protects mice from CVB3-induced viral myocarditis through regulating PKM2/HIF-1α axis mediated metabolic reprogramming of macrophages. *Redox Biol*., **69**: 103016.

Zhang Y, Wang Y, Zhu A, Yu N, Xia J and Li J (2024). Dual-targeting biomimetic semiconducting polymer nanocomposites for amplified theranostics of bone metastasis. *Angew Chem Int Ed Engl*., **63**(2): e202310252.

Zhao XL, Wang SZ, Zhang L, Wang Z, Huang JY, Liao S, Lu M, Yang Z, Zhao XJ, Zhao ZY, Guo ZX, Zhang LN, Zhu PD and Xu M (2024). Mn, N co-doped CDs as a fluorescent nanosensing platform for the detection of tannic acid and hafnium ion and in vitro fluorescence imaging of U2OS osteosarcoma cells. *Mikrochim Acta*., **192**(1): 13.

Zhao Y, Zhang B, Zhang Q, Ma X and Feng H (2021). Tumor-associated macrophages in osteosarcoma. *J Zhejiang Univ Sci B*., **22**(11): 885–892.

Zheng L, Zhuang Z, Li Y, Shi T, Fu K, Yan W, Zhang L, Wang P, Li L and Jiang Q (2021). Bone targeting antioxidative nano-iron oxide for treating postmenopausal osteoporosis. *Bioact Mater*., **14**: 250–261.